Transient Electromagnetic Interference on Buried Pipelines Caused by Double Circuit Overhead Power Lines

T. A. Papadopoulos, A. G. Martins-Britto, A. I. Chrysochos

***Abstract*—Analysis of the electromagnetic interference (EMI) between overhead lines (OHL) and nearby buried pipelines requires the accurate calculation of the self and mutual electrical parameters of all conductors in the arrangement. This becomes more important when investigating high-frequency (HF) EMI. Common approaches presume that the impact of the mutual capacitive coupling as well as the frequency-dependent soil characteristics can be disregarded. However, such approximations may result into estimates that overlook critical interactions. In this article, a recent formulation for calculating both the mutual impedance and admittance between overhead and underground conductors is adopted to investigate HF EMI on a pipeline caused by lightning strikes in a double-circuit OHL. Wave propagation characteristics and transient responses are computed using both frequency-dependent and constant properties soil models to evaluate the importance of the proposed approach on EMI studies; significant differences are observed. Comparisons are also carried out with approximate earth formulations, where the influence of the dispacement current is disregarded. In addition, the impact of the pipeline burial depth is examined.**

***Keywords*—Earth conduction effects, electromagnetic transients, mutual admittance, overhead lines, pipelines, underground conductors.**

I. Introduction

INDUCED voltages due to electromagnetic (EM) coupling between overhead power lines (OHLs) and neighboring metallic facilities, such as pipelines has long been recognized as a significant challenge in shared right-of-way corridors. The growing use of joint energy corridors, aimed at minimizing environmental impact and optimizing space, has intensified the need for accurate electromagnetic interference (EMI) assessments. Such interference results from the coupling of electric and magnetic fields, inducing voltages and currents in adjacent metallic structures that can compromise the safety and integrity of infrastructure, particularly pipelines [1]–[3]. High induced voltages may lead to safety hazards, including electric shock, insulation degradation, and corrosion, thus impacting both personnel safety and the longevity of the pipeline infrastructure [4]–[8].

Past studies have primarily addressed EMI under steady-state and fault conditions, focusing on low-frequency (LF) scenarios and employing classical methods such as Carson's equation [9] and its subsequent extensions, including Pollaczek's impedance formulas for underground systems [10]. These models, however, do not represent properly high-frequency (HF) effects, where frequency-dependent (FD) soil characteristics and displacement currents become more pronounced [11]–[15]. A recent work has shown that as EMI studies extend into the HF spectrum, the currently employed approximations often produce estimates that may overlook critical interactions, particularly when poorly conductive soils are involved [7], [12].

One common assumption in EMI modeling of OHL/pipeline configurations is the presumed negligible impact of mutual capacitive coupling, often due to the perceived shielding effect of the conductive earth [16], [17]. Recent formulations indicate that, contrary to prevailing beliefs, mutual admittance plays a non-trivial role in accurately characterizing HF-induced voltages on pipelines [18], [19], even in the cases where coupling occurs between overhead and underground conductors [20].

In a previous work [20], the authors introduced new expressions for calculating the mutual impedance and admittance between OHLs and buried pipelines, demonstrating that mutual admittance can be significant in HF EMI scenarios and must not be disregarded. Building on this foundation, the present study extends the investigation to a double-circuit OHL configuration, examining the complex impacts of FD soil properties on transient-induced voltages. A detailed case study, where an underground pipeline shares the same right-of-way with a 110 kV double-circuit OHL, is presented.

This paper further elucidates how the soil frequency-dependence contributes to transient EMI responses, particularly regarding displacement current effects involving overhead and underground conductors (i.e., OHL in close proximity with a buried pipeline). The influence of soil resistivity and conductor depth in the power line modes are analyzed with a focus on the propagation characteristics across different soil conditions. The impact of earth displacement current and eventually of the mutual capacitive coupling is also demonstrated with transient induced voltage calculations on the pipeline. This study advances EMI research by providing new insights on mode characterization of double-circuit lines under EMI conditions, and introduces a refined approach for transient

T. A. Papadopoulos is with the School of Electrical & Computer Engineering, Aristotle University of Thessaloniki, 54124, Thessaloniki Greece, (e-mail: thpapad@ece.auth.gr).

Amauri G. Martins-Britto is with KU Leuven, division Electa & the Etch Competence Hub of EnergyVille, Genk, Belgium. (e-mail: amauri.martinsbritto@kuleuven.be).

Andreas I. Chrysochos is with R&D Department, Hellenic Cables, Maroussi, 15125 Athens, Greece (e-mail: achrysochos@hellenic-cables.com).

Paper submitted to the International Conference on Power Systems Transients (IPST2025) in Guadalajara, Mexico, June 8-12, 2025. This work is partially supported by the Etch Competence Hub of EnergyVille, financed by the Flemish Government.

analysis in shared energy corridors.

II. Mutual Impedance and Admittance Formulas

The configuration shown in Fig. 1 represents an overhead, i, and an underground conductor, j. The EM parameters of air, namely, permittivity, permeability and conductivity are ϵ_0, μ_0, σ_0, and of the homogeneous earth are denoted as ϵ_1, μ_1 and σ_1. In this aspect, the propagation constants of air and earth with respect to $\omega = 2\pi f$ are defined as:

$$\gamma_k = \sqrt{j\omega\mu_k(\sigma_k + j\omega\epsilon_k)}. \tag{1}$$

with the subscript k taking values 0 and 1 for air and earth, respectively.

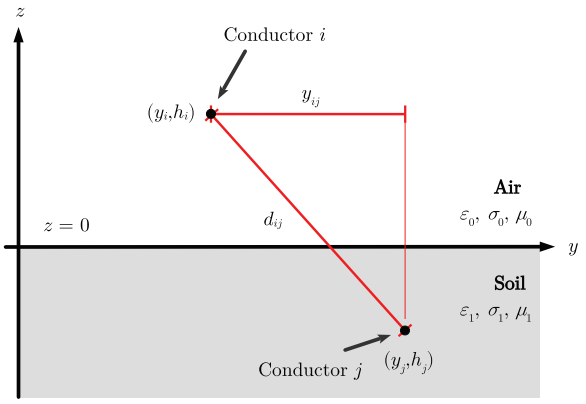

Fig. 1. Parallel thin conductors located in the air and earth.

The formulas for the mutual impedance and the mutual potential coefficient between the overhead and the underground conductors are in the general form of (2) and (3), respectively [20]:

$$Z_{eij} = Z_{eij} = \frac{j\omega\mu_0\mu_1}{\pi}\int_0^\infty \frac{e^{(-a_0h_i+a_1h_j)}}{(a_0\mu_1+a_1\mu_0)}\cos(\lambda y_{ij})d\lambda, \tag{2}$$

$$P_{eij} = P_{eij} = \frac{-\omega^2\mu_0\mu_1}{\pi} \times \int_0^\infty \frac{(a_0\mu_0+a_1\mu_1)e^{(-a_0h_i+a_1h_j)}}{(a_1\mu_1\gamma_0^2+a_0\mu_0\gamma_1^2)(a_0\mu_1+a_1\mu_0)}\cos(\lambda y_{ij})d\lambda. \tag{3}$$

where, $a_k = \sqrt{\lambda^2+\gamma_k^2+k_x^2}$ and $k_x = 0$. The complex semi-infinite integrals of (2) and (3) are evaluated numerically via the vectorized adaptive quadrature method [21].

Considering multiconductor configurations, the total per-unit-length (pul) impedance, $\boldsymbol{Z_{tot}}$, and admittance, $\boldsymbol{Y_{tot}} = j\omega\boldsymbol{P_{tot}^{-1}}$, matrices are formulated on the basis of [19], including proper terms regarding the skin effect and the coated conductor insulation. Note that, $\boldsymbol{P_{tot}}$ is the total potential coefficient matrix. In particular, regarding the influence of earth, the earth impedance and potential coefficients of conductors located in air are calculated on the basis of [13], [22] and those buried underground by means of [23]. Eventually, $\boldsymbol{Z_{tot}}$ and $\boldsymbol{Y_{tot}}$ are obtained by assembling the self and mutual terms of the air and earth media, as well as their mutual couplings [20].

III. Case Study

A. OHL-pipeline system configuration

A 110 kV double-circuit OHL/pipeline interference case study [24] is investigated to evaluate the propagation characteristics and the transient induced voltages on the pipeline. The cross-section of the system is illustrated in Fig. 2. The underground pipeline shares the same right-of-way with the OHL, with a separation distance of 25 m. A detailed description of the electrical and geometrical parameters of the OHL and the pipeline can be found in [24]. The OHL/pipeline parallel routing (ℓ) is variable, equal to 100 m or 1000 m. The burial depth (d) of the pipeline in the homogeneous soil also varies taking values of 0.5 m, 1 m and 3 m.

B. Circuit modeling

All conductors are assumed to extend outside the parallel region without EMI exposures and groundings; this in terms of circuit analysis refers to an OHL/pipeline system being nearly matched [3], [4], [11], [25]. The system matching is implemented by applying characteristic impedance terminations, namely, 600 Ω impedances at phase conductors, 660 Ω at the shield wire and 80 Ω at the pipeline. Considering the above, the resulting equivalent circuit model of Fig. 3 is defined.

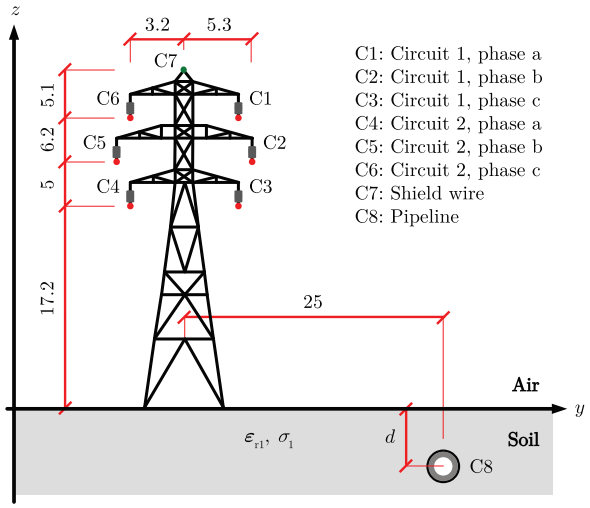

Fig. 2. Lateral view of the OHL/pipeline configuration under study; all dimensions given in meters unless specified otherwise.

The OHL/pipeline system is energized with a 1.2/50 μs double exponential voltage source of 1 p.u. amplitude, to simulate lightning surges. The source is applied to the sending end of the OHL phase a conductor at t = 0 s, as shown in Fig. 3. The transient responses are computed using the frequency-domain transmission line model of [26].

C. Soil models

Several models have been proposed for the prediction of the frequency-dependence of soil electrical properties, ϵ_{r1} and σ_1 with excitation frequency [27]–[29]. In this study, the Longmire and Smith (LS) [29] and the CIGRE (CG) WG C4.33 [28] soil models are examined.

For the LS soil model, the variation of ϵ_{r1} and σ_1 with respect to frequency is predicted by [29]:

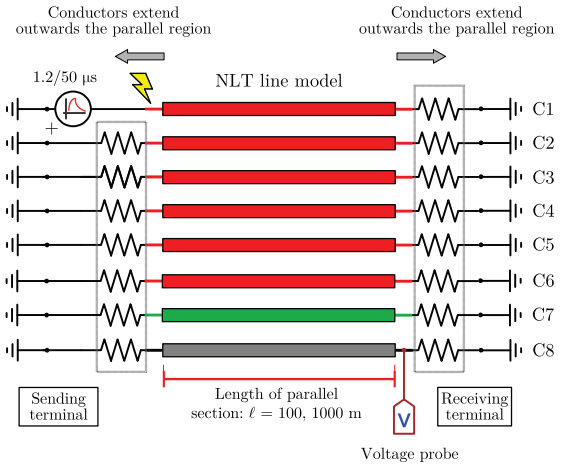

Fig. 3. Equivalent circuit of the parallel routing under study.

$$\epsilon_{r1}(f) = \epsilon_{r1,\infty} + \sum_{n=1}^{13} \frac{a_n}{1 + (f/f_n)^2}, \tag{4}$$

$$\sigma_1(f) = \sigma_{1,DC} + 2\pi f \epsilon_0 \sum_{n=1}^{13} \frac{a_n f/f_n}{1 + (f/f_n)^2}, \tag{5}$$

where $\epsilon_{r1,\infty}$ is the HF relative permittivity of soil (equal to 5 according to [29]), a_n are coefficients given in [29], and f_n are scaling coefficients calculated as a function of the DC soil conductivity, $\sigma_{1,DC}$:

$$f_n = 10^{n-1}(125\sigma_{g,DC})^{0.8312}. \tag{6}$$

For the CG model the corresponding expressions are [28]:

$$\epsilon_{r1}(f) = 12 + 9.5 \cdot 10^4 \sigma_{1,LF}^{0.27} f^{-0.46}, \tag{7}$$

$$\sigma_1(f) = \sigma_{1,LF} + 4.7 \cdot 10^{-6} \sigma_{1,LF}^{0.27} f^{0.54}, \tag{8}$$

where $\sigma_{1,LF} = 1/\rho_{1,LF}$ is the soil conductivity at 100 Hz.

In this study, six FD and three constant properties (CP) soil cases are examined. For the CP cases $\rho_1 = 1/\sigma_1 = 100\ \Omega m$ and $1000\ \Omega m$, with $\epsilon_{r1} = 15$, and $\epsilon_{r1} = 5$, respectively. Accordingly, for the FD LS and CG cases $\rho_{1,LF} = \rho_1$. In Fig. 4 the variation of ρ_1 and ϵ_{r1} with respect to frequency is plotted for the LS and CG soil models. It is apparent that, ρ_1 and ϵ_{r1} decrease with frequency for both FD models. Nevertheless, the CG soil model yields a more pronounced decrease of resistivity with frequency.

IV. Modal Propagation Characteristics

Wave propagation in a N-conductor arrangement is described by the N modes of propagation [30] corresponding to the eigenvalues of the matrix product $\boldsymbol{Y_{tot}Z_{tot}}$, while $\boldsymbol{T_i}$ is the frequency-dependent eigenvector matrix. Thereby, the six aerial phase conductors and the shield wire along with the underground pipeline of Fig. 2 are mapped to eight decoupled modes of propagation, numbered from #1 to #8 [30]. The calculated modal attenuation constant and velocity are presented

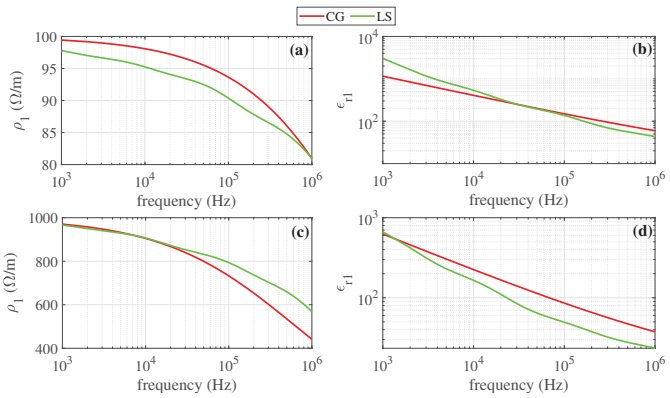

Fig. 4. Soil electrical properties predicted by the LS and the CG soil models. (a), (b) ρ_1 and ϵ_{r1} for $\rho_{1,LF} = 100\ \Omega m$, respectively, and (c), (d) the corresponding variation of ρ_1 and ϵ_{r1} for $\rho_{1,LF} = 1000\ \Omega m$.

with respect to frequency in Figs. 5 and 6, respectively; CP soil with $\rho_1 = 1000\ \Omega m$ and $d = 1\,m$ is examined. For the mode decomposition the Levenberg–Marquardt algorithm has been used [31].

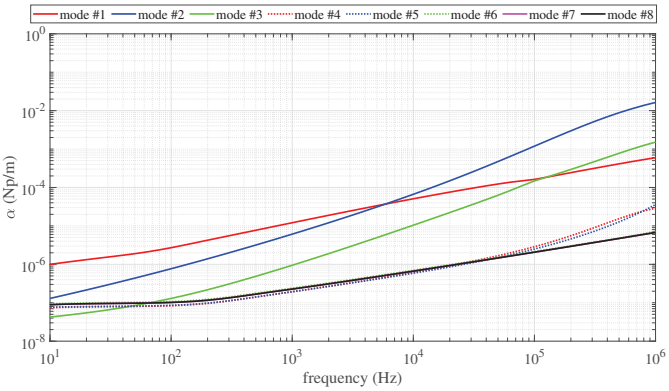

Fig. 5. Mode attenuation constant for CP soil model with $\rho_1 = 1000\ \Omega m$.

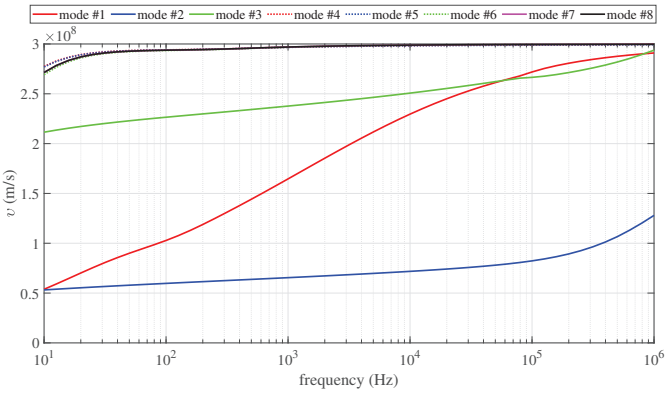

Fig. 6. Mode velocity for CP soil model with $\rho_1 = 1000\ \Omega m$.

To identify the nature of the modes with respect to the OHL/pipeline physical characteristics, the elements of $\boldsymbol{T_i}$ are analyzed as shown in Fig. 7. Subplots of Fig. 7 contain the magnitudes of the elements of the corresponding column of $\boldsymbol{T_i}$. Indices m and n in the figure legends refer to the

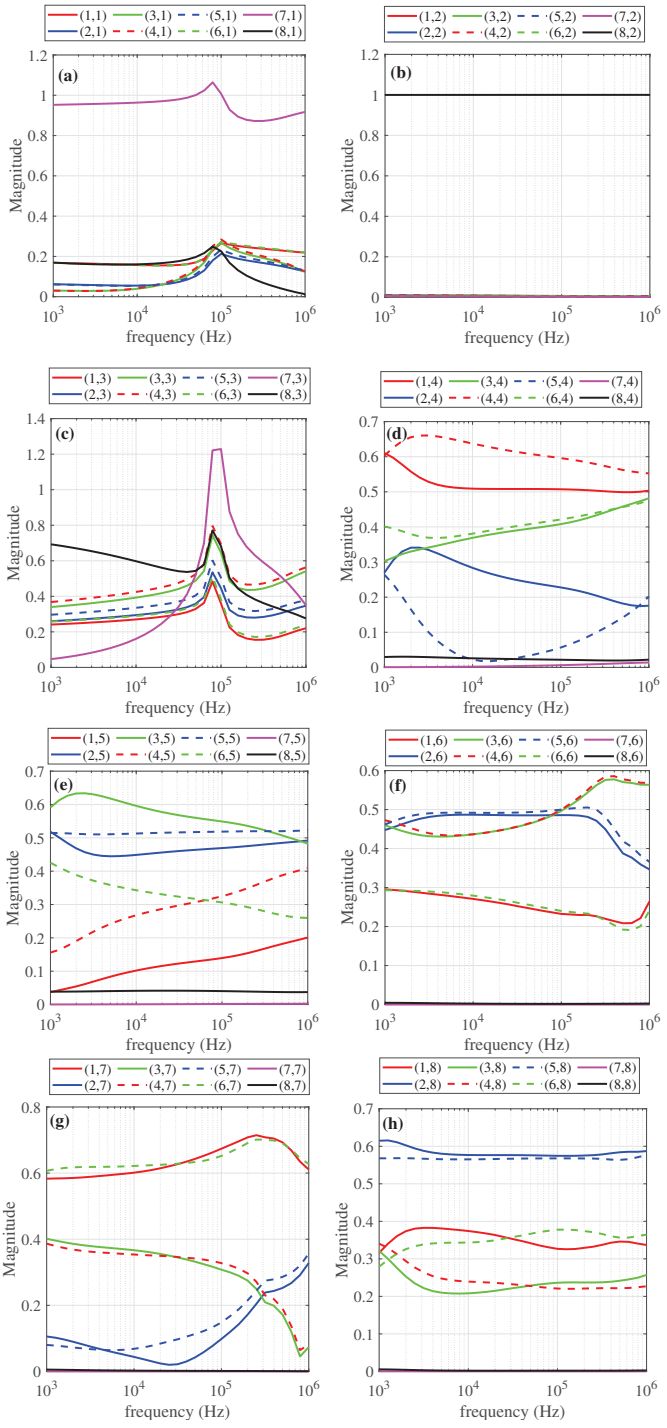

Fig. 7. Modal transformation matrix magnitude of (a) mode #1, (b) mode #2, (c) mode #3, (d) mode #4, (e) mode #5, (f) mode #6, (g) mode #7, (h) mode #8.

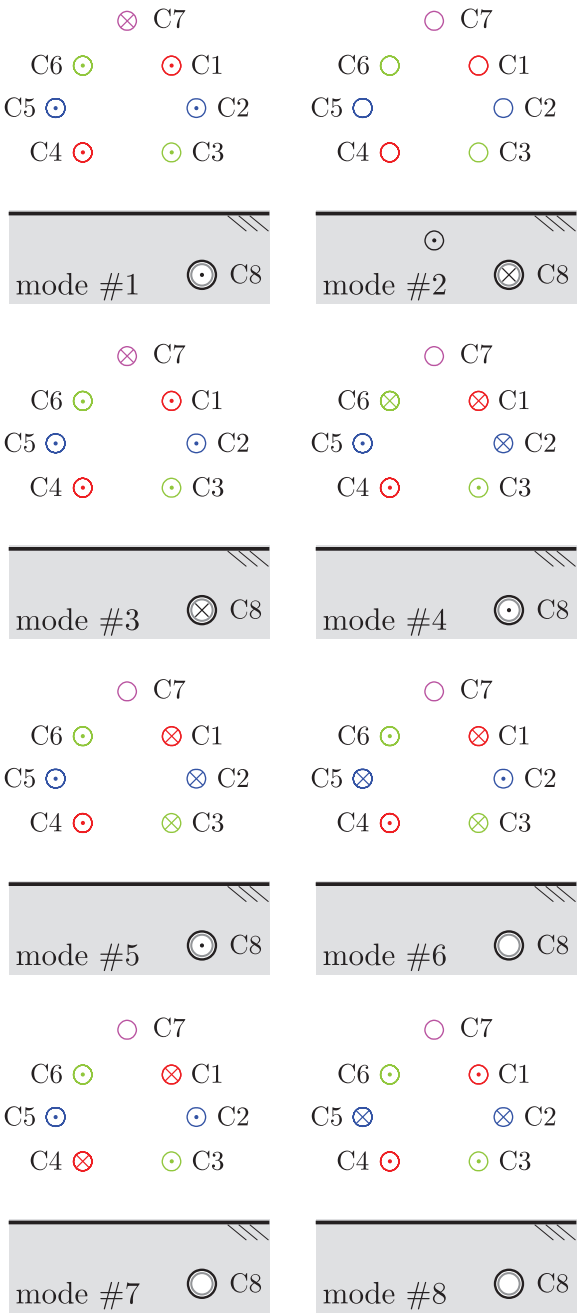

Fig. 8. Source excitation and return currents for propagation modes #1 to #8 at 10 kHz. Symbol ⊗ denotes unit current flow inwards the plane of the paper, and ⊙ represents the opposite.

rows and columns, of matrix $\boldsymbol{T_i}$, respectively. Note that the rows of $\boldsymbol{T_i}$ are related to the conductors of the OHL/pipeline configuration with the numbering as labeled in Fig. 2, e.g., row 1 corresponds to conductor C1, etc.; the columns are related with the modes of propagation, enumerated from #1 to #8. Therefore, each subplot of Fig. 7 can be used to describe the relation of each mode of propagation with the physical characteristics of the OHL/pipeline configuration. These relations are illustrated in Fig. 8, representing the excitation and return currents predominant in each propagation mode at 10 kHz.

From Figs. 5-8, four main groups of modes of propagation can be identified. The first group contains modes #4, #5, #6, #7 and #8, that can be characterized as aerial modes presenting low attenuation and high velocities (see Fig. 5 and Fig. 6) that approach the free-space speed of light with increasing frequency. This is also substantiated by Figs. 7(d)-(h), where these modes correspond to current loops in which the current is injected into one or more phase conductors and returning from

the rest of them. For modes #4 and #5 a small current flow in the pipeline (C8) can be also identified. Mode #3 is analyzed in Fig. 7(c). It shows that particularly for this mode the elements of $\boldsymbol{T_i}$ are frequency dependent. At the LF region (i.e., below 50 kHz), mode #3 can be characterized as a pure pipeline mode. As frequency increases the influence of the sky wire becomes gradually pronounced, converting mode #3 into both a sky wire and pipeline mode. Mode #2 is energized by injecting current into the pipeline (C8) and returns from the ground. As a result, mode #2 can be identified as the ground mode and presents the highest attenuation and the lowest velocity among all modes of propagation. Mode #1 is energized by injecting current into the sky wire (C7) and extracting it from the remaining conducting media. Therefore, this mode is associated mainly with the sky wire and presents high attenuation and slow velocity, particularly at the LF region.

V. Influence of the Burial Depth

The influence of the burial depth on the pipeline propagation characteristics is investigated, by assuming pipeline burial depths of 0.5 m, 1.0 m and 3.0 m. The CP soil model with $\rho_1 = 1000\ \Omega m$ is considered. In Fig. 9 the attenuation constant and velocity of modes #2 and #3 are presented as according to the analysis of the previous section; the influence of the pipeline characteristics is mainly identified in these modes.

It is shown that mode #2 attenuation constant and phase velocity decrease with respect to the burial depth. Differences between the three burial depth cases are marked for frequencies higher than 100 kHz. This behavior of mode #2 is the result of the combined effect of the EM characteristics of the imperfect soil and the pipeline coating [32]. Note that, less substantial variations in the propagation characteristics are identified in mode #3.

The above remarks are also verified in the transient responses of the OHL/pipeline, computed for the different burial depths. In Figs. 10 and 11, the induced voltage at the pipeline receiving end is presented for 100 m and 1000 m parallel routing, respectively. Evidently, the induced pipeline voltage decreases with the burial depth. Differences in the peak of the waveforms are more pronounced for the short parallelism length of 100 m. This is attributed to the fact that as the length of the parallelism decreases, the frequency context characterizing the transient response shifts to higher frequencies, where differences in mode #2 propagation characteristics for the different burial depths are higher, as shown in Fig. 9 [27], [33]. Moreover, the shorter the parallelism length the narrower the pulse becomes, due to the higher frequency context. Results also show that for increasing length of parallelism, the magnitude of the induced voltage increases driven by inductive coupling, which is generally the predominant coupling mechanism [11].

VI. Influence of Soil Properties

To demonstrate the impact of the soil properties on the OHL/pipeline propagation characteristics, comparisons are carried out considering the soil cases described in section III, namely 100 Ωm and 1000 Ωm. The modal propagation

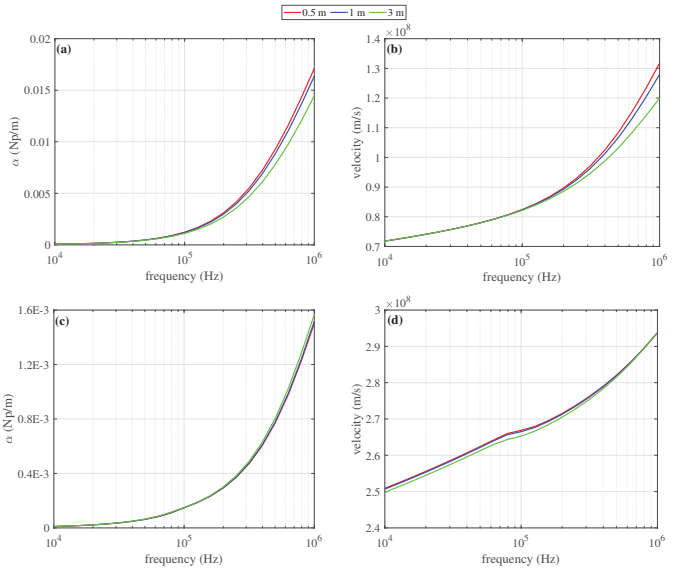

Fig. 9. Modal attenuation constant and velocity of (a), (b) mode #2, and (c), (d) mode #3 with respect to burial depth.

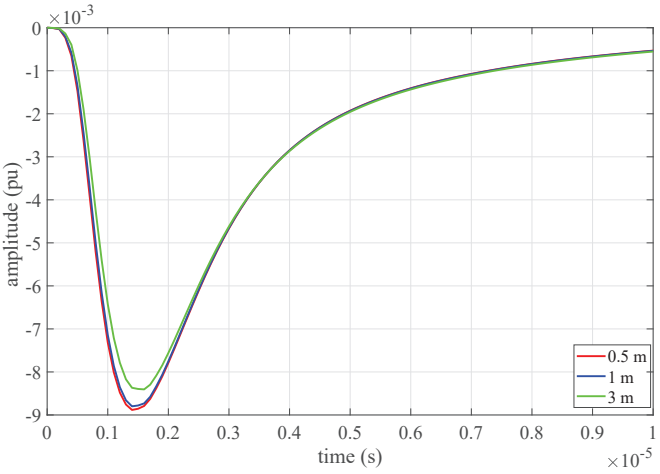

Fig. 10. Transient induced voltages at the pipeline receiving end of a 100-m OHL/pipeline parallel routing for different burial depths; $\rho_1 = 1000\ \Omega m$.

parameters, i.e., attenuation constant, $\alpha(f)$, and velocity, $\upsilon(f)$, of the two FD soil models, $p(f)_{\text{FD soil model}}$, are normalized with respect to the corresponding of the CP soil model results, $p(f)_{\text{CP soil model}}$, as follows:

$$p(f)_{norm} = \frac{p(f)_{\text{FD soil model}}}{p(f)_{\text{CP soil model}}} \tag{9}$$

The normalized propagation characteristics for modes #2 and #3 are summarized in Figs. 12 and 13, respectively, with respect to frequency.

Results for the three soil models are essentially equal at the LF spectrum range. However, as the frequency increases, discrepancies between the FD soil models and the CP one become more marked for increasing resistivity values, especially for the estimation of the attenuation constant, $\alpha(f)$ [7], [27]. This is because the decrease of the soil resistivity and the influence of displacement currents (and eventually ϵ_{r1}) are more

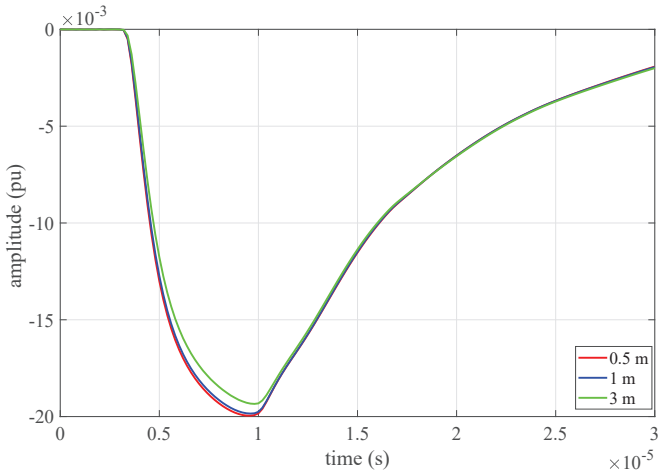

Fig. 11. Transient induced voltages at the pipeline receiving end of a 1000-m OHL/pipeline parallel routing for different burial depths; $\rho_1 = 1000\ \Omega m$.

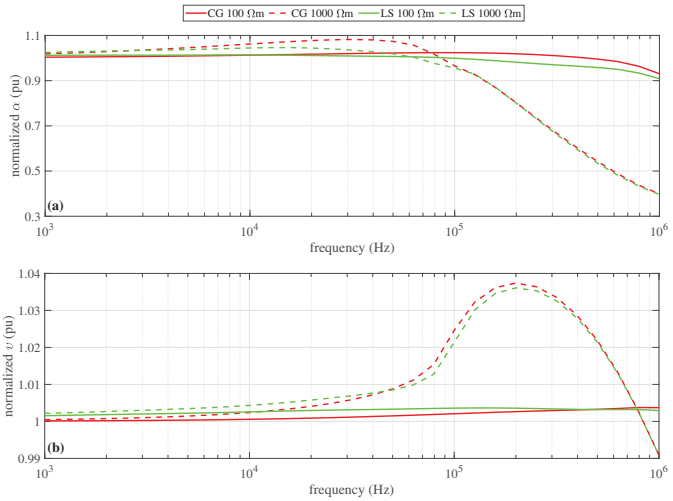

Fig. 13. Normalized mode #3 (a) attenuation constant and (b) velocity for different soil models and electrical properties.

enhanced with increasing frequency in such soil cases. Conversely, for highly conductive soil cases ($\rho_{1,LF} = 100\ \Omega m$), earth behaves as a conductor and conductive currents prevail; thus the effect of ϵ_{r1} on the propagation characteristics is minimal.

Comparing the results obtained with the two FD soil models, it is shown that the LS and the CG soil models yield generally similar results in the examined frequency range. A slightly increased influence of the CG model is observed at the HF region of the frequency spectrum, due to the lower resistivity values predicted by this soil model (see Fig. 4).

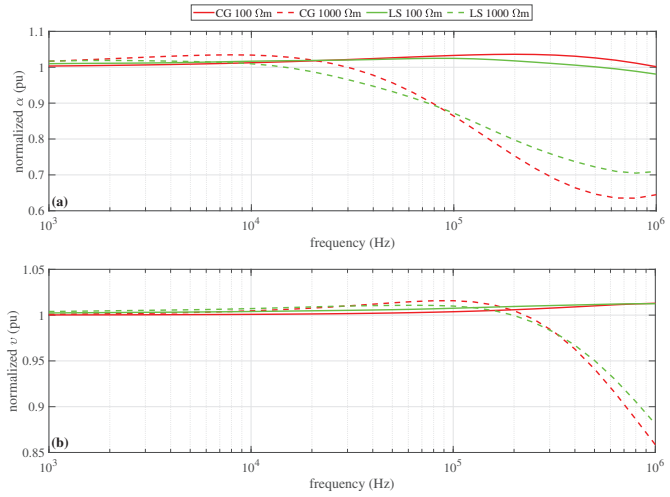

Fig. 12. Normalized mode #2 (a) attenuation constant and (b) velocity for different soil models and electrical properties.

The impact of the soil models is also illustrated in the transient responses of Figs. 14-17, where the induced voltage at the pipeline receiving end is presented for different parallel routing lengths and soil resistivities, employing all soil models.

From Figs. 14 and 15, it can be deduced that the CP soil model presents higher induced voltage compared to the two FD ones. The effect of the latter is more pronounced in Fig. 15 compared to Fig. 14, yielding almost double induced voltage, which is justified by the increased resistivity value. The impact of the parallel routing length is also evident in Figs. 14-17. Generally, for longer parallelism lengths, the soil models exhibit small differences and only for high soil resistivity values as shown in Fig. 17. Conversely, for shorter lengths, characterized by higher frequency context, differences are observed for both soil cases.

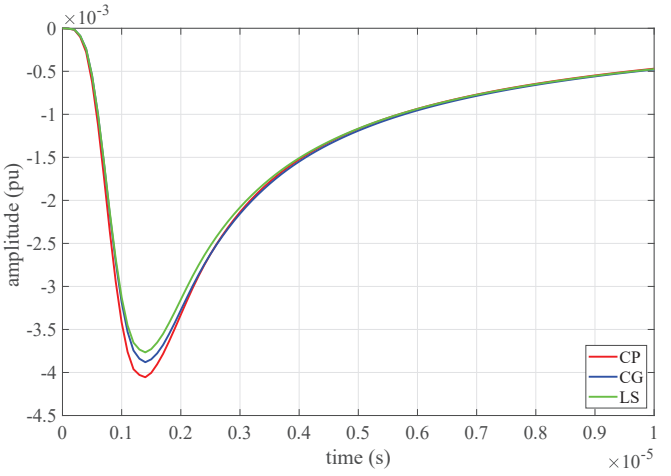

Fig. 14. Transient induced voltages at the pipeline receiving end of a 100-m OHL/pipeline parallel routing for $\rho_1 = 100\ \Omega m$.

VII. Effect of Earth Displacement Current

The transient responses in Fig. 18 provide further analysis of earth displacement currents considering the three FD models under discussion. A comparison is made between the generalized earth admittance formulation described in (3) and the "classical transmission line (TL)" approach, i.e., $\epsilon_1 = 0$ and $P_{eij} = 0$, meaning that earth displacement current is neglected and the conductive earth is assumed to shield the underground pipeline from mutual capacitive couplings with the overhead conductors [16].

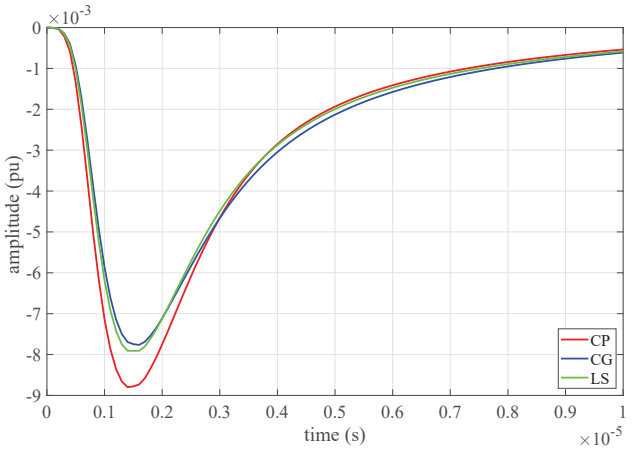

Fig. 15. Transient induced voltages at the pipeline receiving end of a 100-m OHL/pipeline parallel routing for $\rho_1 = 1000\ \Omega m$.

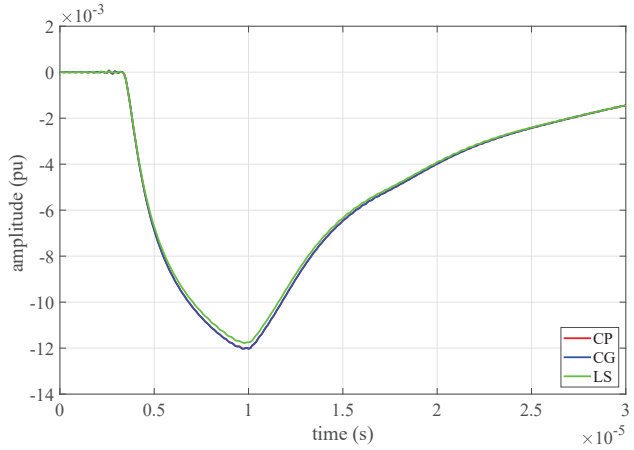

Fig. 16. Transient induced voltages at the pipeline receiving end of a 1000-m OHL/pipeline parallel routing for $\rho_1 = 100\ \Omega m$.

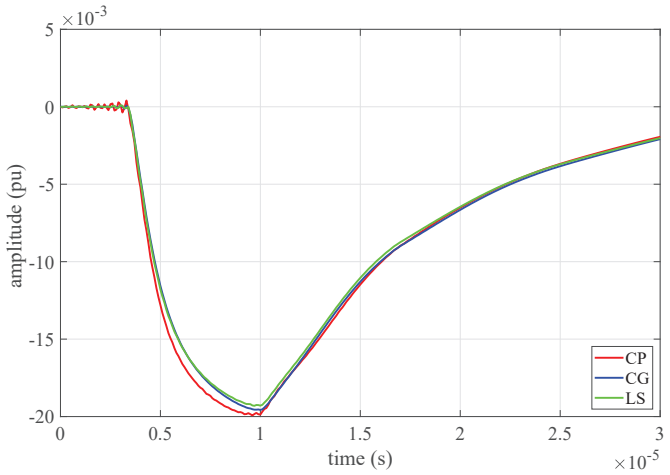

Fig. 17. Transient induced voltages at the pipeline receiving end of a 1000-m OHL/pipeline parallel routing for $\rho_1 = 1000\ \Omega m$.

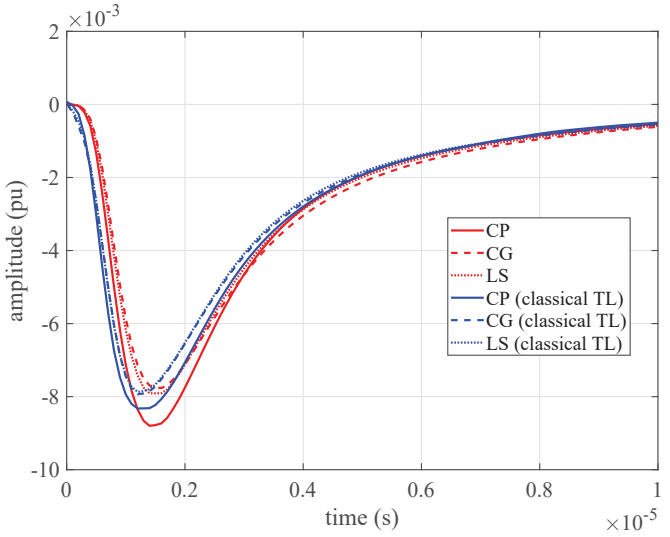

Fig. 18. Effect of the earth impedance formulation on induced voltages at the pipeline receiving end of a 100-m OHL/pipeline parallel routing for $\rho_1 = 1000\ \Omega m$.

It can be generally noted that in both earth formulations, the FD models introduce consistent fast-front peak attenuation compared to the corresponding CP counterparts, which is in line with the expected behavior when resistivity and permittivity are reduced, as Fig. 4 confirms. However, there is a noticeable early arrival of the dominant peaks across all "classical TL" cases, with a steeper rate of voltage drop in the generalized formulation, and more gradual returns to the initial conditions. Overall, when the mutual capacitive couplings are represented, the outcomes show greater differentiation between soil models (CP, CG, LS) than in the classical approach. This suggests that properly accounting for displacement currents amplify the effects of soil model selection, making the choice more critical in practical engineering studies towards safety in transmission and pipeline systems.

VIII. Conclusions

The wave propagation characteristics and the transient performance of underground pipelines caused by a nearby double-circuit OHL has been investigated. A generalized formulation for the calculation of the mutual impedance and the mutual admittance between the overhead conductors and the underground pipeline has been adopted to investigate EMI in a wide frequency range up to 1 MHz. Computations were performed by examining constant and frequency-dependent soil electrical properties, considering two widely used frequency-dependent soil models proposed by Longmire and Smith and CIGRE WG C4.33.

Modal analysis has been applied to analyze the OHL/pipeline wave propagation characteristics. Eight decoupled modes of propagation have been identified and their characteristics were related to the physical properties of the configuration. This type of analysis enhances and facilitates further parametric studies to reveal the impact of different parameters.

In this sense the impact of the pipeline burial depth has been also investigated. It was shown that the burial depth has a slight impact on the propagation characteristics and the

induced voltages at the pipeline when transients are present on the OHL.

From the comparison of propagation characteristics and transient responses with the FD soil models against those of the CP soil model, it was shown that the FD electrical properties of the soil are important at higher frequencies, especially for high resistivity values and shorter lengths of parallelism. The latter is related to the higher frequency context, leading to higher frequency components. Hence, FD soil models should be taken into account in HF EMI investigations of buried pipelines involving such cases. This is especially true when considering the generalized formulation taking into account the mutual coupling between the OHL and the underground pipeline, as the classical TL approach shows a less pronounced sensitivity to the dispersion of the soil electrical properties.

REFERENCES

[1] D. Tsiamitros, G. Christoforidis, G. Papagiannis, D. Labridis, and P. Dokopoulos, "Earth conduction effects in systems of overhead and underground conductors in multilayered soils," *IET Gener. Transm. Distrib.*, vol. 153, pp. 291–299(8), May 2006.

[2] A. Ametani, , T. Yoneda, Y. Baba, and N. Nagaoka, "An investigation of earth-return impedance between overhead and underground conductors and its approximation," *IEEE Trans. Electromagn. Compat.*, vol. 51, no. 3, pp. 860–867, 2009.

[3] I. Cotton, K. Kopsidas, and Y. Zhang, "Comparison of transient and power frequency-induced voltages on a pipeline parallel to an overhead transmission line," *IEEE Trans. Power Del.*, vol. 22, no. 3, pp. 1706–1714, 2007.

[4] *CIGRE WG 36.02. Technical publication n°. 95 - Guide Concerning Influence of High Voltage AC Power Systems on Metallic Pipelines*, 1995.

[5] F. P. Dawalibi, "Modern Computational Methods for the Design and Analysis of Power System Grounding," in *International Conference on Power System Technology*, Beijing, 1998, pp. 122–126.

[6] A. Taflove and J. Dabkowski, "Prediction method for buried pipeline voltages due to 60 Hz AC inductive coupling – Part I: Analysis," *IEEE Trans. Power App. Syst.*, vol. PAS-98, no. 3, pp. 780–787, 1979.

[7] A. G. Martins-Britto, T. A. Papadopoulos, Z. G. Datsios, A. I. Chrysochos, and G. K. Papagiannis, "Influence of lossy ground on high-frequency induced voltages on aboveground pipelines by nearby overhead transmission lines," *IEEE Trans. Electromagn. Compat.*, vol. 64, no. 6, pp. 2273–2282, 2022.

[8] T. Papadopoulos, Z. Datsios, A. Chrysochos, A. Martins-Britto, and G. Papagiannis, "Transient induced voltages on aboveground pipelines parallel to overhead transmission lines," *Electr. Power Syst. Res.*, vol. 223, p. 109631, 2023.

[9] J. Carson, "Wave propagation in overhead wires with ground return," *Bell Syst. Tech. J.*, pp. 539–554, 1926.

[10] F. Pollaczek, "Über das Feld einer unendlich langen wechsel tromdurchflossenen Einfachleitung," *Elect. Nachr. Tech.*, vol. 3, pp. 339–360, 1926.

[11] K. Kopsidas and I. Cotton, "Induced voltages on long aerial and buried pipelines due to transmission line transients," *IEEE Trans. Power Del.*, vol. 23, no. 3, pp. 1535–1543, 2008.

[12] A. G. Martins-Britto, C. M. Moraes, and F. V. Lopes, "Transient electromagnetic interferences between a power line and a pipeline due to a lightning discharge: An EMTP-based approach," *Electr. Power Syst. Res.*, vol. 197, p. 107321, 2021.

[13] W. H. Wise, "Potential coefficients for ground return circuits," *Bell Syst. Tech. J.*, vol. 27, no. 2, pp. 365–371, 1948.

[14] H. Kikuchi, "Wave propagation along an infinite wire above ground at high frequencies," *Electrotech. J. Jpn.*, vol. 2, pp. 73–78, 1956.

[15] T. A. Papadopoulos, G. K. Papagiannis, and D. P. Labridis, "A generalized model for the calculation of the impedances and admittances of overhead power lines above stratified earth," *Electr. Power Syst. Res.*, vol. 80, pp. 1160–1170, 2010.

[16] H. W. Dommel, *EMTP Theory Book*. Bonneville Power Administration, 1986.

[17] J. Morales, H. Xue, J. Mahseredjian, and I. Kocar, "A new tool for calculation of line and cable parameters," *Electr. Power Syst. Res.*, vol. 220, p. 109314, 2023.

[18] T. Papadopoulos, D. Tsiamitros, and G. Papagiannis, "Earth return admittances and impedances of underground cables in non-homogeneous earth," *IET Gener. Transm. Distrib.*, vol. 5, pp. 161–171(10), Feb. 2011.

[19] A. Ametani, "A general formulation of impedance and admittance of cables," *IEEE Trans. Power App. Syst.*, vol. PAS-99, no. 3, pp. 902–910, 1980.

[20] A. G. Martins-Britto, T. A. Papadopoulos, and A. I. Chrysochos, "Transient electromagnetic interference between overhead and underground conductors," *IEEE Trans. Electromagn. Compat.*, vol. 66, no. 3, pp. 983–992, 2024.

[21] L. F. Shampine, "Vectorized adaptive quadrature in MATLAB," *Journal of Computational and Applied Mathematics*, vol. 211, no. 2, pp. 131–140, 2008.

[22] W. H. Wise, "Propagation of high-frequency currents in ground return circuits," *Proc. Inst. Radio Eng.*, vol. 22, no. 4, pp. 522–527, 1934.

[23] T. A. Papadopoulos, D. A. Tsiamitros, and G. K. Papagiannis, "Impedances and admittances of underground cables for the homogeneous earth case," *IEEE Trans. Power Del.*, vol. 25, no. 2, pp. 961–969, 2010.

[24] D. D. Micu, G. C. Christoforidis, and L. Czumbil, "Ac interference on pipelines due to double circuit power lines: A detailed study," *Electric Power Systems Research*, vol. 103, pp. 1–8, 2013.

[25] A. Ametani, "Four-terminal parameter formulation of solving induced voltages and currents on a pipeline system," *IET Science, Measurement & Technology*, vol. 2, pp. 76–87, 2008.

[26] A. I. Chrysochos, T. A. Papadopoulos, and G. K. Papagiannis, "Enhancing the frequency-domain calculation of transients in multiconductor power transmission lines," *Electr. Power Syst. Res.*, vol. 122, pp. 56–64, 2015.

[27] T. A. Papadopoulos, Z. G. Datsios, A. I. Chrysochos, P. N. Mikropoulos, and G. K. Papagiannis, "Wave propagation characteristics and electromagnetic transient analysis of underground cable systems considering frequency-dependent soil properties," *IEEE Trans. Electromagn. Compat.*, vol. 63, no. 1, pp. 259–267, 2021.

[28] "CIGRE WG C4.33. Impact of soil-parameter frequency dependence on the response of grounding electrodes and on the lightning performance of electrical systems," *CIGRE TB 781*, 2019.

[29] C. Longmire and K. Smith, "A universal impedance for soils," *DNA 3788T, Mission Research Corp., Santa Barbara, CA*, 1975.

[30] L. M. Wedepohl, "Application of matrix methods to the solution of travelling-wave phenomena in polyphase systems," *Proc. Inst. Elect. Eng.*, vol. 110, no. 12, pp. 2200–2212, 1963.

[31] A. I. Chrysochos, T. A. Papadopoulos, and G. K. Papagiannis, "Robust calculation of frequency-dependent transmission-line transformation matrices using the Levenberg-Marquardt method," *IEEE Trans. Power Del.*, vol. 29, no. 4, pp. 1621–1629, 2014.

[32] T. A. Papadopoulos, D. A. Tsiamitros, and G. K. Papagiannis, "Analysis of the propagation characteristics of buried cables in imperfect earth," in *2009 IEEE Bucharest PowerTech*, 2009, pp. 1–8.

[33] A. I. Chrysochos, T. A. Papadopoulos, and G. K. Papagiannis, "Rigorous calculation method for resonance frequencies in transmission line responses," *IET Gener. Transm. Distrib.*, vol. 9, pp. 767–778, 2015.